Tracking oxygen atoms in electrochemical CO oxidation – Part I: Oxygen exchange via CO2 hydration

Scott, Søren B.; Kibsgaard, Jakob; Vesborg, Peter C.K.; Chorkendorff, Ib

Published in:
Electrochimica Acta

Link to article, DOI:
10.1016/j.electacta.2021.137842

Publication date:
2021

Document Version
Peer reviewed version

Tracking Oxygen Atoms in Electrochemical CO Oxidation - Part I: Oxygen Exchange via CO_2 Hydration

Soren B. Scott[a,1], Jakob Kibsgaard[a], Peter C. K. Vesborg[a], Ib Chorkendorff[a,*]

[a] *SurfCat Section for Surface Physics and Catalysis, Department of Physics, Technical University of Denmark, 2800 Kgs Lyngby, Denmark*
[b] *Spectro Inlets A/S, Ole Maaløes Vej 3, 2200 København*

Abstract

We report a new method to measure the kinetic rate constant of CO_2 hydration using electrochemical oxidation of carbon monoxide (CO oxidation) in isotope-labeled electrolyte. CO oxidation is often used as a model reaction to investigate the surface of metallic electrocatalysts, most notably in CO stripping experiments. Using chip-based electrochemistry mass spectrometry with ^{18}O-labeled electrolyte we show that: 1) For CO stripping experiments on Pt, one oxygen in the product CO_2 comes from the reactant CO and the other comes from the electrolyte, consistent with the Langmuir-Hinshelwood mechanism involving the adsorbates $^{*}CO$ and $^{*}OH$. 2) Some of the formed CO_2 subsequently exchanges oxygen with the electrolyte via short-lived carbonic acid. We use the time-dependent isotopic ratios to calculate the kinetic reaction rate constant of the CO_2 hydration reaction and compare it to literature. By doing this at two different temperatures we show that the method is robust and that ^{18}O-labeled CO stripping experiments provide an accurate measurement of the rate constant for CO_2 hydration. Chip-based electrochemistry mass spectrometry combined with isotopic labeling is thus shown to be a versatile and powerful tool for elucidating mechanistic aspects of homogeneous reactions as well as electrocatalytic reactions.

Keywords: kinetics, CO2 hydration, CO oxidation, DEMS, mechanisms

1. Introduction

The reaction of carbon dioxide with water to form carbonic acid (CO_2 hydration, Reaction 1) is important both in climate science, where it drives ocean acidification as well as the ocean's ability to take up carbon[1]; and in biology,

*Corresponding author
Email address: ibchork@fysik.dtu.dk (Ib Chorkendorff)

where it plays a major role in respiration and in determining the pH of blood[2].

$$CO_2 + H_2O \leftrightarrow H_2CO_3 \qquad K_{eq} = 1.7 \cdot 10^{-3} \tag{1}$$

This reaction is receiving increasing attention as a necessary step in CO_2 mitigation and utilization strategies including enzyme-assisted CO_2 capture[3, 4] and electrochemical CO_2 reduction[5]. The equilibrium constant heavily favors CO_2, such that CO_2 dissolved in acidic solutions spends only 0.17% of its time as carbonic acid[6]. In near-neutral solutions, carbonic acid is quickly deprotonated to bicarbonate (HCO_3^-), greatly increasing the overall solubility, and Reaction 1 in the forward direction is the rate-limiting step for CO_2 dissolution as HCO_3^-. Only when the pH exceeds 9 does the direct reaction of hydroxide with dissolved CO_2 contribute substantially to the dissolution rate[7]. The rate constant for CO_2 hydration by Reaction 1 is thus the property of interest for most of the applications mentioned above. The rate constant is most commonly measured by stop-flow pH titration[8, 9, 10, 11], but in the past has also been measured by electrical conductivity changes[12], calorimetry[7], and facilitated diffusion[13]. All of these methods require a rather large amount of solution (10's of ml). Here we present a new and versatile method of measuring the rate constant especially suitable to small reaction volumes, 100 μl with the potential to decrease to as small as 2 μl, which enables screening of expensive enzyme or catalyst samples produced initially in very small quantities. The method is centered on quickly generating a controlled amount of CO_2 in an electrochemical setting by oxidation of carbon monoxide (CO) and then monitoring the exchange of oxygen atoms between CO_2 and water.

Electrochemical CO oxidation is itself a reaction of great interest in electrocatalysis. CO adsorbs strongly on noble metal surfaces, and is therefore a poison to the hydrogen electrodes of fuel cells if present in the hydrogen stream[14, 15], and is also a useful experimental probe molecule of electrocatalyst surfaces based on platinum (Pt)[16, 15, 17, 18]. Most commonly, CO stripping experiments are used as a standard method of measuring the electrochemically accessible surface area of noble metal catalysts. The onset of CO electro-oxidation has also been used to infer characteristics of the active surface such as the density of oxyphilic sites[16, 15]. The latter is possible because CO oxidation occurs by a Langmuir-Hinshelwood reaction mechanism, whereby adsorbed $^*CO$ reacts with co-adsorbed $^*OH$.

The new method of observing the interaction of CO_2 and H_2O presented here uses ^{18}O isotope labeling and chip-based electrochemistry - mass spectrometry (EC-MS)[19] to monitor the isotopic distribution of CO_2 produced by electrochemical CO oxidation in real time. This article is the first in a two-part series on the isotopic distribution of CO_2 produced by electrochemical CO oxidation, with the second article focused fully on the reactivity of the electrocatalyst. As such, this first article starts with a detailed look at CO oxidation experiments on Pt.

2. Experimental

2.1. Materials

Electrolyte was prepared by dissolving 7.9 μl of 70% $HClO_4$ (Suprapure, Merck) in 97% $H_2{}^{18}O$ (Medical Isotopes).

CO was 6.0 purity from AGA.

The Pt electrode is a pure polycrystalline Pt stub from MaTeck (99.99%) It was flame-annealed, cooled in argon, and rinsed in milli-Q water (18.2 MΩ cm, Millipore A/S) before use.

2.2. Electrochemistry - mass spectrometry setup

The EC-MS setup is described in detail in Reference [18]. The interface between the liquid test environment and the vacuum chamber of the mass spectrometer is formed by a silicon chip. The internal volume of the chip functions as a microscopic headspace to a thin-layer liquid working volume which transports dissolved volatiles to the mass spectrometer and also saturates the working volume with a carrier gas of choice. The working volume was defined by a 100 μm Teflon spacer and by a stagnant thin-layer cell. The working distance L was slightly more than 100 μm due to sample indentation. The interface and cell were from Spectro Inlets A/S. The electrode potential was controlled with a Biologic SP200 potentiostat, and the setup was equipped with a Balzers QMA 400 mass spectrometer.

The Pt electrode was cycled from 0 to 1.4 V vs RHE for $\geq$ 1 hr before starting experiments, so that the base cyclic voltammogram and the background MS signals were stable.

2.3. Calibration and characterization of the setup

Calibration of mass spec signals was done as described in Reference [20]. For H_2 at m/z=2, O_2 at m/z=32, and CO_2 at m/z=44, signals were calibrated electrochemically, using steady-state hydrogen evolution (HER), oxygen evolution (OER), and (bulk) CO oxidation experiments, respectively. For CO at m/z=28 and He at m/z=4, signals were calibrated semi-externally using the calculated capillary flux.

The working distance L was determined by measuring the limiting hydrogen oxidation on a platinum electrode with H_2 as carrier gas.

The isotopic purity of the labeled electrolyte was also calibrated internally, using the isotopic distribution of the O_2 produced by OER. The isotopic purity is described by the parameter α, defined as:

$$\alpha = \frac{c_{H_2{}^{16}O}}{c_{H_2{}^{16}O} + c_{H_2{}^{18}O}} \,. \tag{2}$$

The directly measurable quantity is the ratio of m/z=34 ($^{16}O^{18}O$) to m/z=36 ($^{18}O_2$) signal during OER, γ:

$$\gamma = \frac{S_{M34}}{S_{M36}} \tag{3}$$

The isotopic purity is related to this ratio, according to the binomial distribution, by Equation 4:

$$\alpha = \frac{\gamma}{2+\gamma}\,. \tag{4}$$

This is described in more detail in the Supporting Information (SI).

2.4. Data treatment

The data and analysis and plotting scripts for this work are available at https://github.com/ScottSoren/pyCOox_public. The scripts make use of the open-source `ixdat` python package (https://ixdat.readthedocs.io).

3. Results and Discussion

3.1. CO oxidation in electrolyte containing $H_2^{18}O$

Figure 2 shows results for electrochemical oxidation of CO on polycrystalline Pt in 0.1 M $HClO_4$ made with water which is 97% $H_2{}^{18}O$. Apart from the isotopic label, the experiments are completely analogous to those which we presented previously in Figure 3 of Reference [18].

Starting from the left of Figure 2a, the electrode black trace in the bottom panel) is scanned back and forth while the electrode is in He-saturated electrolyte. At the cathodic potential, 0.010 V vs the reviersible hydrogen electrode (V_{RHE}), H_2 is observed as a m/z=2 signal. At the most anodic potential, 1.7 V_{RHE}, oxygen is evolved, as seen in the m/z=36 and m/z=34 signals, corresponding to $^{18}O_2$ and $^{16}O^{18}O$, respectively. This gives an internal measurement of the isotopic purity of the electrolyte, as described in the Experimental section according to Equation 4. The electrolyte in this experiment has an impurity of $\alpha = 5.6\%$ $H_2{}^{16}O$. The first full cyclic voltammagram in He, starting and ending in the double layer region on the anodic scan, as indicated by the yellow highlight, is shown as Cycle 1 with solid lines in Figure 1b.

Just before $t = 400$ s, as the potential scans through the double layer region in the cathodic direction, the gas in the chip is abruptly switched from He to CO. When the potential reaches the cathodic limit ca 10 seconds later, no hydrogen is evolved, indicating that the CO has saturated the electrolyte and poisoned the electrode surface. During the subsequent anodic scan, an anodic current wave starts with an initial spike and falls to a more stable level while the mass spectrometer signals at m/z=46, m/z=48, and m/z=44, corresponding to $C^{16}O^{18}O$, $C^{18}O_2$, and $C^{16}O_2$, respectively, grow. This is attributed to CO oxidation, with ^{18}O coming from the electrolyte. The OER signals at m/z=34 and 36 for the first anodic CV apex in CO, at 500 s, resemble the two cycles in He, whereas the OER signals for the second anodic turn in CO are lower, most likely due to a loss of undercoordinated sites due to the tendency of CO to increase the mobility of atoms on the Pt surface and anneal out defects[16]. The first full cyclic voltammagram in CO, indicated by the green highlight, is shown as Cycle 3 with dashed lines in Figure 2b.

Figure 2c shows a CO stripping experiment. Starting from the left, a cycle from +0.035 to +1.200 V_{RHE} probes the state of the electrode. Despite the cathodic potential being more positive than the standard equilibrium potential for HER/HOR, there is a net production of H_2, leading to the m/z=2 signal in the mass spectrometer. Though this is a nominal underpotential for HER, hydrogen production is consistent with thermodynamics (Nernst equation) because the electrolyte is far from saturated with hydrogen. The anodic limit is not sufficiently positive to evolve oxygen, but a small CO_2 signal is discernible from the background at m/z=48 and 46. This CO_2 signal prior to introduction of CO represents a tiny fraction of a monolayer, significantly smaller than the signals we focus on in this article, and is approximately constant from cycle to cycle in base cyclic voltammetry and between experiments (see, e.g., our previous work[18]). We attribute it to unidentified organic residues which are present in the electrolyte or on the electrode. After this initial cycle, the potential is held constant at +0.4 V_{RHE}, in the double-layer region, and CO is dosed through the chip from approximately 225 s to 275 s. Right when CO is dosed, there a cathodic current transient, the CO displacement current[15]. After switching back to He, a few minutes are allowed to pass for the CO signal to return to background, and then two complete cyclic voltammagrams are recorded with the same potential range as the initial cycle, starting with a cathodic sweep. No hydrogen is observed on the first cycle, indicating that the electrode surface is completely poisoned. During the first anodic sweep, there is a transient anodic current coinciding with the appearance of mass spectrometer signals at m/z=46, m/z=48, and m/z=44. This first cyclic voltammagram after the dose, indicated by the yellow highlight, is replotted against potential as Cycle 6 in Figure 2d. The scan rate used in these experiments, 20 mV/s, the same as Figure 3 of ref. [18], is relatively high, making the tails of the CO2 signals more pronounced when projected onto a potential axis. The second cycle after the CO dose, indicated by the green highlight and replotted as Cycle 7 in Figure 2d, resembles the initial cycle prior to the CO dose, indicating the electrode surface has been fully cleaned.

The oxidation of *CO on polycrystalline Pt is characterized by a sudden onset at ≈0.7 V in electrolyte saturated with inert gas (Figure 2d) and ≈0.85 V_{RHE} in CO-saturated electrolyte (Figure 2b). In both cases, the onset is much higher than the equilibrium potential[6] for CO oxidation of -0.1 V_{RHE}. This is a special case of the inverted relationship between CO oxidation activity and CO partial pressure which led early on to the insight that a co-adsorbate is needed for *CO oxidation, i.e. that it follows the Langmuir-Hinshelwood mechanism[21]. Specifically, *CO poisons the surface against its own oxidation by taking up all the free metal sites and blocking the co-adsorbate, taken to be *OH. This conclusion has been supported by numerous electrochemical and in-situ spectroscopy studies since then, as summarized by Marc Koper in ref. [15]. When the reaction involves labeled electrolyte ($H_2{}^{18}O$) and un-labeled CO

($C^{16}O$), then the mechanism can be written as follows:

$$C^{16}O + * \longrightarrow *C^{16}O \tag{5}$$

$$H_2{}^{18}O + * \longrightarrow *{}^{18}OH + (H^+ + e^-) \tag{6}$$

$$*C^{16}O + *{}^{18}OH \longrightarrow C^{16}O^{18}O + 2* + (H^+ + e^-) \tag{7}$$

Thus, the product CO_2 should ideally be exclusively of the $C^{16}O^{18}O$ isotope, detected by the mass spectrometer at m/z=46. In reality, the electrolyte has an impurity of $H_2{}^{16}O$, measured to be 5.6%, as described above, and the CO has the natural isotopic distribution, meaning an 0.2% $C^{18}O$ impurity. While the observed m/z=44 ($C^{16}O_2$) signal can be explained by the isotopic impurity in the electrolyte, the observed m/z=48 ($C^{18}O_2$) signal, ≈22% of the total CO_2 signal, is much too large to be explained by the isotopic impurity of the CO. The $C^{18}O_2$ signal thus implies CO_2 with both oxygens originating from the electrolyte. Given that Pt is not predicted to dissociate the strong triple bond in CO[22, 15], we attribute this to exchange of oxygen between CO_2 and H_2O in the electrolyte.

3.2. Mass transport of CO_2

If CO_2 hydration is responsible for the m/z=48 signal, then this theory should be able to explain why it has a different shape than the signals at m/z=44 and m/z=46.

The shape of mass spectrometer signals in chip EC-MS can normally be explained by the mass transport of electrochemical products in the setup: namely (1) diffusion from the electrode to the chip membrane, and then (2) evaporation and gas-phase flow through the capillary to the vacuum chamber. These two steps contribute the two terms of the characteristic response time for CO_2 in the system, given by[23, 18]

$$\tau = \frac{L^2}{2D^{CO_2}} + \frac{LA_{el}p}{\dot{n}^0 K_H^{CO_2}} = 4.4\,\mathrm{s} + 10.4\,\mathrm{s} = 14.8\,\mathrm{s}, \tag{8}$$

where $L = 130\,\mu$m is the working distance, $D^{CO_2} = 1.9 \cdot 10^{-9}$ m^2/s is the diffusion constant of CO_2 in water, $A_{el} = 0.196$ cm^2 is the electrode area, $p = 1$ bar is the pressure in the chip, $\dot{n}^0 = 8.6$ nmol/s is the total capillary flux through the chip, and $K_H^{CO_2} = 28$ bar/M is the Henry's Law volatility constant of CO_2 in water. This characteristic response time is what makes the signals for CO_2 ($\tau = 14.8$ s) in Figure 2 much broader than the signals for H_2 ($\tau = 2.1$s) or O_2 ($\tau = 4.4$ s).

In figure 3 we compare the expected shape of the CO_2 response based on this mass transport model to the observed signals at m/z=44, 46, and 48 in the experiment shown in Figure 2a.

In the top panel of Figure 3, the CO oxidation current is estimated by ΔJ, the excess anodic current in Cycle 2 of Figure 2 compared to Cycle 1 during both the anodic and cathodic potential sweeps. This excess anodic current is

characterized by a slow onset right after the double-layer region ($t = 0$ in Figure 3); a spike as the oxidadation of the adsorbed CO layer is ignited, a steady region; and then a fall to near zero at the anodic turn ($t \approx 65$ s in Figure 3), where the fully oxidized surface is deactivated for CO oxidation[16, 15] and the two CV's coincide in the OER region. The CO oxidation current increases again during the cathodic scan as the surface regains activity, with a small spike in activity as the potential crosses ≈ 0.7 V_{RHE} ($t \approx 115$ s in Figure 3) on the cathodic scan. Note that using ΔJ as the CO oxidation current implicitly assumes that the cathodic reduction wave in Cycle 1 is merely hidden in cycle 2 by a CO oxidation current of the opposite sign.

The CO oxidation current ΔJ is taken as the input to a mass-transport model simulating the diffusion of CO_2 in the working volume electrolyte and the evaporation of CO_2 across the membrane of the chip [23]. The CO_2 concentration resulting from the model is shown as a function of time (horizontal axis) and distance from the membrane of the chip (y, vertical axis). The electrode is separated from the membrane by a working distance of $y_{max} = L = 132\,\mu$m, as determined from the mass-transport limited HOR current, as described in the Experimental Section Figure S1. The transport of CO_2 is limited by its high solubility, and thus low equilibrium vapor pressure in the chip's sampling volume[18], and therefore CO_2 builds up to an extent in the working volume electrolyte.

The expected CO_2 flux to the mass spectrometer is proportional to the simulated concentration of CO_2 at the membrane of the electrode, and can thus be derived from the model results. The simulated CO_2 flux is shown in the bottom panel, plotted together with the normalized measured signal for the three CO_2 isotopes. While the shape of the signals for $C^{16}O_2$ (m/z=44) and $C^{16}O^{18}O$ (m/z=46) closely match the expected shape based on the mass transport model, the shape of the $C^{18}O_2$ (m/z=48) signal is significantly slower - i.e., broadened and shifted towards the right. The same trailing behavior in the $C^{18}O_2$ signal is clear in the CO stripping experiment in Figure 2c-d.

We hypothesize that the delay of the $C^{18}O_2$ signal compared to the other CO_2 signals is due to the slowness of the CO_2 hydration reaction. Though the $C^{18}O_2$ molecules are separated in time from the $C^{16}O^{18}O$ and $C^{16}O_2$ molecules, it is not a *separation process* in the traditional understanding - the effect is not due to doubly labeled CO_2 molecules taking longer to reach the mass spectrometer than singly labeled molecules. Instead the effect results from random processes giving CO_2 molecules a wide range of residence times and the fact that the longer a CO_2 molecule is dissolved in labeled water, the more likely it is to have both of its oxygen atoms labeled.

3.3. Kinetic model of oxygen exchange

According to our hypothesis, the m/z=48 signal is due to $C^{18}O_2$ formed when CO_2 is hydrated and then the resulting carbonic acid dissociates to water and CO_2 again, but with the oxygen atoms exchanged between the molecules. Because most of the CO_2 is initially $C^{16}O^{18}O$ and the solvent contains mostly

$H_2{}^{18}O$, the most important exchange reaction in this experiment is:

$$C^{16}O^{18}O + H_2{}^{18}O \xrightarrow{k} H_2C^{16}O^{18}O_2 \xrightarrow{1/3\,k2} H_2{}^{16}O + C^{18}O_2 \qquad (9)$$

Here, k is the rate constant for the hydration reaction, and $k_2 = {}^{k}/_{K_{\mathrm{eq}}}$ is the rate constant for the dissociation reaction. Since $K_{\mathrm{eq}} \ll 1$, the dissociation rate constant is much faster than the hydration rate constant ($k_2 \gg k$), and to a good approximation, a molecule of carbonic acid dissociates instantly when formed. However, it makes sense to assume that the oxygen atoms in the carbonic acid molecule are indistinguishable, such that there is no "memory" of which oxygen atoms came from CO_2 and which came from H_2O. This is reasonable because, although two oxygen atoms in carbonic acid are protonated and the third instead has a double bond to the carbon, proton-exchange reactions and electronic relaxations are much faster even than k_2. We also assume that there is no isotopic effect. Together, these assumptions give rise to the factor $1/3$ before k_2 in Reaction 9: the carbonic acid could expel any one of its three oxygen atoms as water, but must expel the ^{16}O in order for the hydration+dissociation event to result in an isotopic exchange.

The value of the un-catalyzed CO_2 hydration rate constant is reported as a function of temperature in Reference [9], which uses a pH-static technique (titration-based) and also compiles previous values for the un-catalyzed kinetics of carbon dioxide hydration. At the standard temperature of 25° C, the hydration rate constant is $k = 0.037\ \mathrm{s}^{-1}$.

Reaction 9 is only one of eight possible hydration + dissociation reactions occurring through a molecule of carbonic acid containing both ^{16}O and ^{18}O. All eight reactions are indicated schematically in Figure 4a. Reaction 9 is the bottom-most reaction path in the scheme. The overall rate of Reaction 9 is

$$r_9 = \frac{1}{3}ka(H_2{}^{18}O)a(C^{16}O^{18}O) = \frac{1}{3}k(1-\alpha)c_{\mathrm{M46}}\,, \qquad (10)$$

where $a(H_2{}^{18}O) = (1-\alpha)$ is the activity of labelled water, which is equivalent to its mol fraction assuming no isotope effects; and $a(C^{16}O^{18}O) = c_{\mathrm{M46}}$ is the activity of singly-labeled CO_2, which is equivalent at these low concentrations to the concentration of $C^{16}O^{18}O$ divided by 1 M.

Because all of the reactions are first-order in CO_2 concentration, we can simplify the picture by dividing by the total CO_2 concentration. Neglecting small isotope effects in mass spectrometer sensitivity, the partial concentration is equal to the partial MS signal, defined as

$$\hat{c}_{\mathrm{M46}} = \hat{s}_{\mathrm{M46}} = \frac{s_{\mathrm{M46}}}{s_{\mathrm{M44}} + s_{\mathrm{M46}} + s_{\mathrm{M48}}}\,, \qquad (11)$$

and likewise for $C^{16}O_2$ (M44) and $C^{18}O_2$ (M48).

Adding the effects of the eight reactions represented in Figure 4a, the expected of change of the partial signals is captured in the following matrix equa-

tion:

$$\frac{\mathrm{d}}{\mathrm{d}t}\begin{pmatrix}\hat{s}_{\mathrm{M44}}\\ \hat{s}_{\mathrm{M46}}\\ \hat{s}_{\mathrm{M48}}\end{pmatrix} = k\begin{pmatrix}-\frac{2}{3}(1-\alpha) & \frac{1}{3}\alpha & 0\\ \frac{2}{3}(1-\alpha) & -\frac{1}{3} & \frac{2}{3}\alpha\\ 0 & \frac{1}{3}(1-\alpha) & -\frac{2}{3}\alpha\end{pmatrix}\begin{pmatrix}\hat{s}_{\mathrm{M44}}\\ \hat{s}_{\mathrm{M46}}\\ \hat{s}_{\mathrm{M48}}\end{pmatrix} \tag{12}$$

To test this, we just need to follow the relative intensities at for an experiment in which the initial CO_2 concentrations, $\underline{\hat{\mathbf{c}}}_0 = \underline{\hat{\mathbf{s}}}_0$, is known. The CO stripping experiment in Figure 2c-d approximates just such an experiment. All of the CO is stripped off in a matter of less than ≈ 5 s, and the resulting CO_2 slowly escapes through the chip thereafter, with the signals not fully returning to baseline for $\approx$100 s. During that time, some of it exchanges oxygen with the water in the electrolyte. Assuming the carbon-oxygen bond in CO is never dissociated on platinum, the CO_2 resulting directly from the oxidation of the monolayer of $^{*}CO$ is has $C^{16}O_2$ and $C^{16}O^{18}O$ in the same ratio as $H_2{}^{16}O$ and $H_2{}^{18}O$ in the electrolyte, and negligible $C^{18}O_2$. In vector form, the initial condition is

$$\begin{pmatrix}\hat{s}_{\mathrm{M44}}\\ \hat{s}_{\mathrm{M46}}\\ \hat{s}_{\mathrm{M48}}\end{pmatrix}_0 = \begin{pmatrix}\alpha\\ 1-\alpha\\ 0\end{pmatrix}. \tag{13}$$

The CO stripping experiment from Figure 2c-d is re-plotted in Figure 4b with partial CO_2 signals in the upper panel. The peak CO oxidation current is used to define $t=0$. The result of the kinetic model defined by Equations 12 and 13 are co-plotted as dotted lines.

The model fits the data more or less perfectly with the rate constant from the literature. Another experiment was done with $T = 35°$ C (Figure S2). Here the evolution of the isotopic distribution is best fit with $k = 0.080$ s^{-1}, which is exactly the value of k given for 35° C in Reference [9]. The experiment was repeated several times at both 25°C and 35°C with high reproducibility. Thus our experiment provides independent verification of the literature rate constants for the CO_2 hydration reaction using a completely different measurement approach.

An important point to note is that for this model to provide an accurate fit, the reaction can't proceed too quickly or too slowly. Specifically, the characteristic time of the reaction has to be comparable to the amount of time the CO_2 spends in the labeled water. For the uncatalyzed hydration at 25 C, the characteristic time is $1/k = 27$ s, and with the working distance and chip capillary used in this article, the characteristic time of mass transport is $\tau = 15$ s, fulfilling this condition. For a medium containing a catalyst, the characteristic time of CO_2 hydration may be significantly faster, and so a balance would need to be met between dilution of the catalyst and speeding up the mass transport by decreasing the working distance or using a chip with a higher capillary permeability. However, we also note that matching of the characteristic time of the reaction to the residence time in the electrolyte can be done (within perhaps an order of magnitude) by changing the spacer thickness - i.e. changing the distance between the working electrode and the gas permable membrane. which strongly affects the residence time.

All in all, the reported approach demonstrates a new and useful way of measuring the rate of CO_2 hydrogenation that could also be used in, e.g., a solution containing a CO_2 hydration catalyst such as the carbonic anhydrase enzyme[2], and perhaps the method could be extended to other hydration reactions as well.

4. Conclusion and Outlook

In this report, we examine the origin of the oxygen atoms in CO_2 detected after electrochemical oxidation of CO in electrolyte containing water labeled with the ^{18}O oxygen isotope. We show that for CO_2 produced by CO oxidation on platinum, one oxygen atom comes from the CO and the other from the electrolyte, resulting primarily in a $C^{16}O^{18}O$ signal at m/z=46 as expected. However, interaction of CO_2 with water via short-lived carbonic acid (H_2CO_3) results in isotopic scrambling. In the time that it takes CO_2 to diffuse through the electrolyte towards the mass spectrometer, a substantial portion of it exchanges the ^{16}O atom inherited from the CO reactant with ^{18}O fom the electrolyte and is observed as $C^{18}O_2$ at m/z=48. Tracking the rate of this isotopic conversion gives an accurate way to measure the rate of CO_2 hydrogenation, as we demonstrate by comparing the observed CO_2 isotopic distribution against that predicted by a kinetic model. The method succeeds in determining the uncatalyzed rate constant for CO_2 hydration at 25 C and 35 C in agreement with traditional titration-based methods.

CO_2 hydrogenation is a very important reaction in both life and climate sciences, and we think that this method constitutes a new way to study CO_2 hydrogenation catalysts such as the carbonic anhydrase enzyme. The method depends on the characteristic times of CO_2 hydration (27 s uncatalyzed at room temperature) and CO_2 transportation to the mass spectrometer (15 s in the present study) being of the same order of magnitude, though these can be tuned by dilution of the catalyst or adjusting the working distance, respectively. In addition to electrochemical CO oxidation, it is also possible to eliminate the electrocatalyst and introduce CO_2 directly to a labeled electrolyte via the interface chip, with a slight modification of the kinetic and mass transport models. Beyond CO_2 it is probable that the method can be generalized to other hydration reactions; and more generally, that the method provides a new means of measuring the rate constant of any reaction that (i) releases a gas, and (ii) can be triggered by an electrode or the introduction of a gas. Exploration of all the possibilities is beyond the scope of the present work.

Accounting for the exchange of oxygen between CO_2 and H_2O is also necessary when investigating other isotope effects in electrochemical CO oxidation. In the second article of this two-part series, we focus on the electrocatalyst, and extend beyond platinum to iridium and oxides of these two noble metals.

5. Competing interests

The authors have no competing interests to declare.

6. Acknowledgments

This work was supported by the Villum Foundation VSUSTAIN Grant 9455 to the Villum Center for the Science of Sustainable Fuels and Chemicals.

References

[1] Intergovernmentntal Panel on Climate Change and Intergovernmental Panel on Climate Change. Climate Change 2014: Synthesis Report. Technical report, United Nations, 2014.

[2] Joseph Feher. Acid–Base Physiology I. In *Quantitative Human Physiology*, chapter 6.5, pages 665–671. Elsevier, Feher2017, 2017.

[3] Claudio Greco, Vincent Fourmond, Carole Baffert, Po Hung Wang, Sébastien Dementin, Patrick Bertrand, Maurizio Bruschi, Jochen Blumberger, Luca De Gioia, and Christophe Léger. Combining experimental and theoretical methods to learn about the reactivity of gas-processing metalloenzymes. *Energy and Environmental Science*, 7(11):3543–3573, 2014.

[4] Dong Kook Park and Man Sig Lee. Kinetic study of catalytic CO2 hydration by metal-substituted biomimetic carbonic anhydrase model complexes. *Royal Society Open Science*, 6(8), 2019.

[5] Stephanie A Nitopi, Erlend Bertheussen, Søren B. Scott, Xinyan Liu, K Albert, Sebastian Horch, Brian Seger, Ifan E. L. Stephens, Karen Chan, Jens K. Nørskov, Thomas F. Jaramillo, and Ib Chorkendorff. Progress and Perspectives of Electrochemical CO 2 Reduction on Copper in Aqueous Electrolyte. *Chemical Reviews*, page DOI: 10.1021/acs.chemrev.8b00705, 2019.

[6] W M Haynes, Thomas J Bruno, and David R Lide, editors. *Handbook of Chemistry and Physics, 96th Edition*. CRC Press, 96 edition, 2015.

[7] B R W Pinsent, L Pearson, and F J W Roughton. The kinetics of combination of carbon dioxide with hydroxide ions. *Transactions of the Faraday Society*, 1(1512):1512–1520, 1956.

[8] Raja G. Khalifah. The Carbon Dioxide Hydration Activity of Carbonic Anhydrase. *J. Biol. Chem.*, 246(8):2561–2573, 1971.

[9] Kenneth S Johnson. Carbon dioxide hydration and dehydration kinetics in seawater. *Limnology and Oceanography*, 27(5):849–855, 1982.

[10] Xiaoping Zhang and Rudi van Eldik. A Functional Model for Carbonic Anhydrase: Thermodynamic and Kinetic Study of a Tetraazacyclododecane Complex of Zinc(II). *Inorganic Chemistry*, 34(22):5606–5614, 1995.

[11] Lucas Koziol, Carlos A. Valdez, Sarah E. Baker, Edmond Y. Lau, William C. Floyd, Sergio E. Wong, Joe H. Satcher, Felice C. Lightstone, and Roger D. Aines. Toward a small molecule, biomimetic carbonic anhydrase model: Theoretical and experimental investigations of a panel of zinc(II) aza-macrocyclic catalysts. *Inorganic Chemistry*, 51(12):6803–6812, 2012.

[12] R. N. J. Saal. The velocity of ionic reactions, II. *Recueil des Travaux Chimiques des Pays-Bas*, 47(4):264–285, sep 2010.

[13] Terrence L Donaldson and J. A. Quinn. Kinetic Constants Determined from Membrane Transport Measurements: Carbonic Anhydrase Activity at High Concentrations. *Proceedings of the National Academy of Sciences*, 71(12):4995–4999, dec 1974.

[14] J J Baschuk and Xianguo Li. Carbon monoxide poisoning of proton exchange membrane fuel cells. *International Journal of Energy Research*, 25(8):695–713, 2001.

[15] Marc T M Koper, Stanley C S Lai, and Enrique Herrero. Mechanisms of the Oxidation of Carbon Monoxide and Small Organic Molecules at Metal Electrodes. *Fuel Cell Catalysis*, pages 159–207, 2009.

[16] K. J.J. Mayrhofer, M. Arenz, B. B. Blizanac, V. Stamenkovic, P. N. Ross, and N. M. Markovic. CO surface electrochemistry on Pt-nanoparticles: A selective review. *Electrochimica Acta*, 50(25-26 SPEC. ISS.):5144–5154, 2005.

[17] Eleonora Zamburlini, Kim D Jensen, Ifan E L Stephens, Ib Chorkendorff, and María Escudero-Escribano. Benchmarking Pt and Pt-lanthanide sputtered thin films for oxygen electroreduction: fabrication and rotating disk electrode measurements. *Electrochimica Acta*, 247:708–721, 2017.

[18] Daniel B Trimarco, Soren B Scott, Anil H Thilsted, Jesper Y Pan, Thomas Pedersen, Ole Hansen, Ib Chorkendorff, and Peter C.K. Vesborg. Enabling real-time detection of electrochemical desorption phenomena with sub-monolayer sensitivity. *Electrochimica Acta*, 268:520–530, apr 2018.

[19] Daniel B. Trimarco. *Real-time detection of sub-monolayer desorption phenomena during electrochemical reactions: Instrument development and applications*. Phd thesis, Technical Unviersity of Denmark, 2017.

[20] Soren B Scott. *Isotope-Labeling Studies in Electrocatalysis for Renewable Energy Conversion, and the Net Carbon Impact of this PhD Project*. Phd, Technical University of Denmark, 2019.

[21] S Gilman. The Mechanism of Electrochemical Oxidation of Carbon Monoxide and Methanol on Platinum. II. The "Reactant-Pair" Mechanism for Electrochemical Oxidation of Carbon Monoxide and Methanol 1. *The Journal of Physical Chemistry*, 68(1):70–80, jan 1964.

[22] Glenn Jones, Jon Geest Jakobsen, Signe S. Shim, Jesper Kleis, Martin P. Andersson, Jan Rossmeisl, Frank Abild-Pedersen, Thomas Bligaard, Stig Helveg, Berit Hinnemann, Jens R. Rostrup-Nielsen, Ib Chorkendorff, Jens Sehested, and Jens K. Nørskov. First principles calculations and experimental insight into methane steam reforming over transition metal catalysts. *Journal of Catalysis*, 259(1):147–160, 2008.

[23] Soren B. Scott. *Investigating the Electrochemical Reduction of Carbon Dioxide using In Situ Mass Spectrometry.* Master's thesis, Technical University of Denmark, 2016.

7. Figures

Figures come at the end, accoring to author guide.

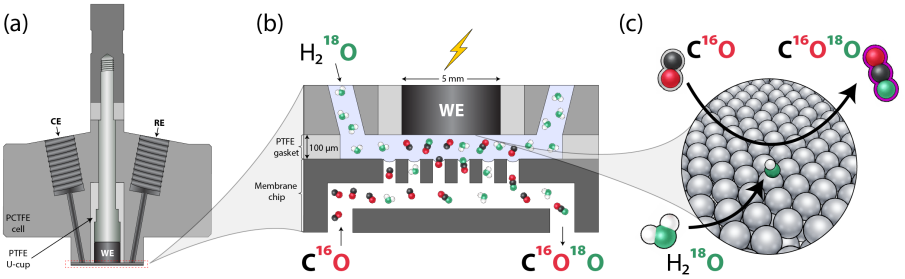

Figure 1: The chip-based electrochemistry mass spectrometry setup. **a** shows the top part of the assembly which accomodates all electrical connections and the ports for introducing (and removing) electrolyte, **b** is a cross-sectional close-up of the heart of the system, namely the working electrode (WE) surface above a thin layer of electrolyte above the surface of the chip with the gas-permeable membrane, which connects directly to the mass spectrometer, **c** artist's impression of the reaction of unlabeled CO with ^{18}O-labeled H_2O forming mixed isotope CO_2.

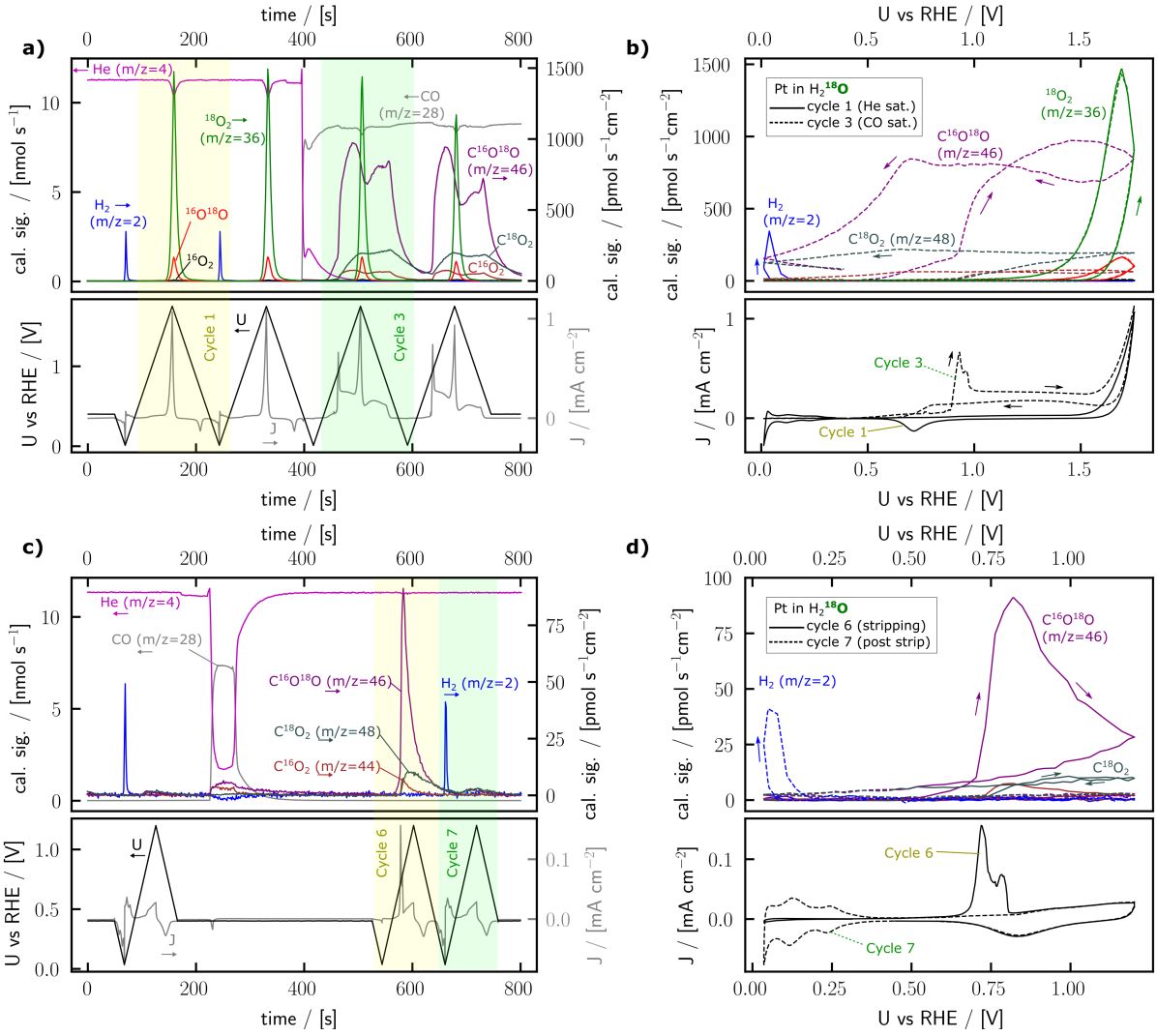

Figure 2: CO oxidation on a polycrystalline platinum electrode in labeled electrolyte (0.1 M $HClO_4$ in 94.4% $H_2{}^{18}O$). Bulk CO oxidation (**a** and **b**) and CO stripping experiments (**c** and **d**) are plotted in two ways: (a and c) As EC-MS plots. Here, electrochemical potential and current are in the bottom panel and calibrated mass spectrometric signals are in the top panel, and the two panels share a time axis. Arrows indicate which axis values are plotted on. (b and d) Against potential. The data from the cycles indicated with yellow and green highlights are re-plotted with potential on the x-axis. Arrows indicate the direction of the potential scan. All scans are 20 mV/s.

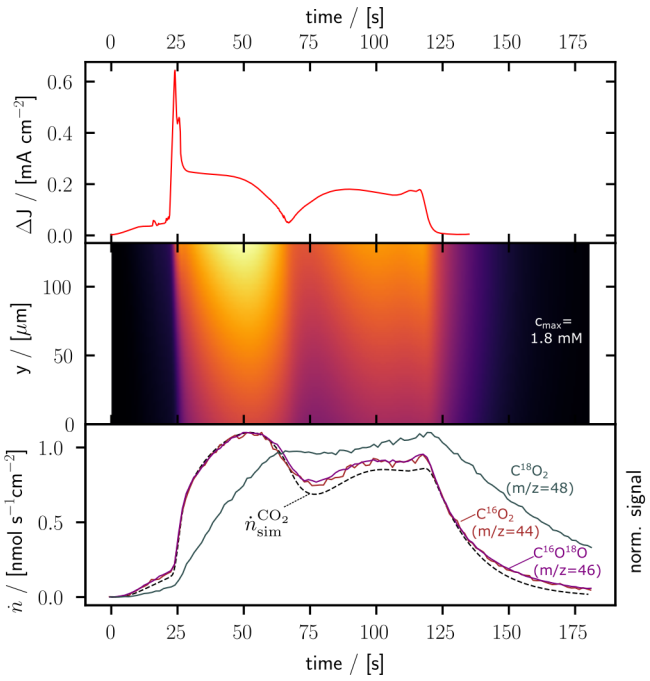

Figure 3: Mass transport model for electrochemically produced CO_2 in ^{18}O-labeled 0.1 M $HClO_4$. Top: the expected CO_2 production rate at the electrode surface, obtained by subtracting the current in cycle 2 from that in cycle 1 of Figure 2. Middle: the calculated CO_2 concentration in the working electrolyte volume as a function of time (x-axis) and distance from the membrane interfacing with the vacuum chamber of the mass spectrometer (y-axis). The electrode surface is 132 μm from the membrane (determined by limiting HOR current). Bottom panel: the expected flux ($\dot{n}_{\mathrm{sim}}^{\mathrm{CO_2}}$, black dotted line, left y-axis) compared to the normalized measured fluxes of $C^{16}O_2$, $C^{16}O^{18}O$, and $C^{18}O_2$ (right y-axis).

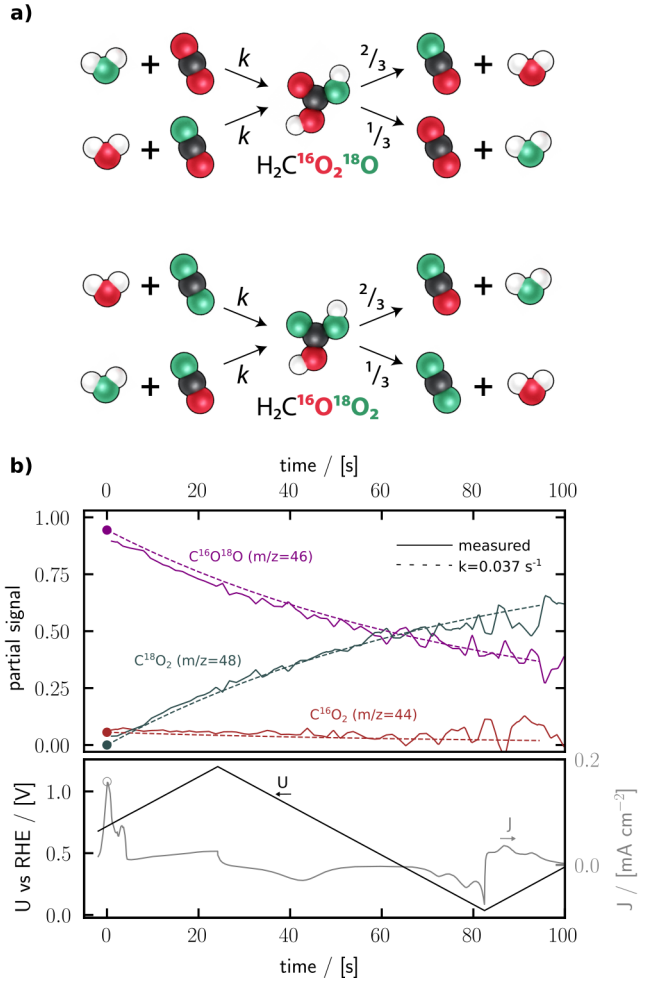

Figure 4: Determination of the rate constant for CO_2 hydrogenation based on a CO stripping experiment in ^{18}O-labeled 0.1 M $HClO_4$. **(a)** Sketch of the possible oxygen-exchanging reactions between CO_2 and H_2O. Black is carbon, white is hydrogen, red is ^{16}O, and green is ^{18}O. **(b)** Zoom-in on the CO stripping experiment from Figure 2c showing, in the upper panel, a comparison of the measured isotopic distribution (solid lines) to that expected (dashed lines) based on the kinetic model described in the text.